Compression failure and fiber-kinking modeling of laminated composites

A. Kabiri Ataabadi*[1], S. Ziaei-Rad[1], and H. Hosseini-Toudeshky[2]

[1]*Department of Mechanical Eng., Isfahan University of Technology, Isfahan 84156-83111, Iran*
[2]*Department of Aeronatical Eng., Amirkabir University of Technology, Hafez Ave., Tehran, Iran*

(Received August 18, 2010, Revised October 13, 2011, Accepted October 21, 2011)

Abstract. In this study, the physically-based failure models for matrix and fibers in compression and tension loading are introduced. For the 3D stress based fiber kinking model a modification is proposed for calculation of the fiber misalignment angle. All of these models are implemented into the finite element code by using the advantage of damage variable and the numerical results are discussed. To investigate the matrix failure model, purely in-plane transverse compression experiments are carried out on the specimens made by Glass/Epoxy to obtain the fracture surface angle and then a comparison is made with the calculated numerical results. Furthermore, shear failure of $(\pm 45)_s$ model is investigated and the obtained numerical results are discussed and compared with available experimental results. Some experiments are also carried out on the woven laminated composites to investigate the fracture pattern in the matrix failure mode and shown that the presented matrix failure model can be used for the woven composites. Finally, the obtained numerical results for stress based fiber kinking model and improved ones (strain based model) are discussed and compared with each other and with the available results. The results show that these models can predict the kink band angle approximately.

Keywords: laminated composite; compression; fiber-kinking; matrix failure.

1. Introduction

During the recent years, many researches focus on the damage and failure analyses of composite laminates due to the increase of demand for composite structures in the industries. Delamination, matrix compressive failure, fiber compressive failure, matrix tensile failure and fiber tensile failure are typical damages in the composite structures. Investigations on the compressive failure modes of composite materials are not as extensive as the other failure modes. Therefore, a theoretical and experimental understanding of this complex failure mode is required to improve the performance of these materials which is also the aim of the present study.

Initially, Puck and Schurmann (1998 and 2002) proposed a matrix compressive failure model based on the Mohr-coulomb criterion and further developments were later carried out by Davila *et al.* for LaRC02/03 failure criteria (Davila *et al.* 2003 and Davila and Camanho 2003). Pinho (2005) implemented these failure criteria into a finite element code and proposed a modification for the consideration of friction stresses. This modification leads to more conservative failure load predictions.

Depending on the material and geometry, different fiber compressive failure modes, such as micro

* Corresponding author, Ph, D. Student, E-mail: a.kabiriataabadi@me.iut.ac.ir

buckling, kinking and fiber failure may occur in the composite laminates. Some researchers considered the kinking mode as a consequence of micro buckling, while others considered that as a separate failure mode (Schultheisz and Waas 1996, Singh and Kumar 2010). The main focus of this article is on the fiber-kinking damage mode in unidirectional composite laminates. Kinking can be defined as the localized shear deformation of the matrix. In this failure mode which can be localized in a band across a specimen, the fibers are rotated by a large amount and the matrix is usually subjected to a large shear deformation.

Rosen (1965) proposed a 2D mechanical model to describe fiber micro buckling. He obtained the fiber's buckling stresses by minimizing the internal energy. The obtained results by Rosen's model were typically 1.5 times higher for boron/epoxy, 2 to 3 times higher for carbon/epoxy and 4 times higher for glass/epoxy composites when compared with the experimental results. These differences in failure stress prediction may be due to the disregarding of 3D effects as discussed by Lager and June (1969), de Ferran and Harris (1970) and assumption of perfectly straight fibers as mentioned by Schultheisz and Waas (1996). Furthermore, the laminate construction may lead to different fiber arrangements within the plane of the lamina and through the thickness direction. Fiber misalignment angles have first been reported to be smaller in the through the thickness direction comparing with the plane of lamina (Davis 1975), but more recent results reported that they are similar in magnitude (Shuart 1989).

Argon (1972) considered the fiber-kinking as a separate failure mode. He assumed that failure occurs as a result of matrix shear failure by an initial fiber misalignment. Budiansky (1983) later extended Argon's analysis and in an analytical work with Fleck (Budiansky and Fleck 1993), he included the effect of strain hardening, shear loads, kink band inclination and finite fiber stiffness, performing a non closed form solution for failure load prediction.

Kyriakides *et al.* (1995) carried out micro mechanical 2D FE models for the analysis of kinking phenomena, including matrix nonlinear behavior and initial imperfections. Liu *et al.* (2004) considered the effect of random waviness of the fibers using a Cosserat smeared out finite element method.

Budiansky *et al.* (1998) used unidirectional analysis to define two kind of steady state kink propagation of: band broadening, in which an established kink band grows in the direction of loading, and transverse propagation, in which a kink band travels across the width of the composite specimen. Their theoretical study was on the bases of various physical models and included the effects of fiber bending resistance in the analyses.

Christensen and Deteresa (1997) incorporated a simple strain based yield/failure criterion into a kink band analysis of compressive failure. Considering of the real conditions of fiber misalignment they predicted compressive failure loads of about one-fifth of the ideal value and with the kink band inclinations of about 20 deg.

Davila *et al.* (2003), used a combination of Argon's approach and the LaRC02/03 matrix failure criterion. Essentially, Davila *et al.* (2003) supposed that the fibers might be misaligned and that further rotation will occur by applying of the compressive loading. Then they computed the stresses in the updated misalignment frame to check the matrix failure using LaRC02/03 matrix failure criterion.

A 2D and 3D stress based kinking model has also proposed by Pinho (2005). In this model, which is based on Argon's approach and the later developments by Davila *et al.* (2003), the stresses are calculated from the strains in the global coordinate and then they transformed into the misalignment local coordinate to determine the applied shear stress on the fibers. Taking the advantage of the shear constitutive law, increasing of the misalignment angle can be determined. In the misalignment coordinate the matrix failure criteria is checked and if it is satisfied, then the stresses in the kink band are degraded.

In this article, the physically-based failure models for matrix and fibers in compression and tension are implemented into a finite element code. Experiments are also carried out on the woven laminated composites to investigate the fracture patterns in the matrix failure mode. The 3D stress based kinking model is also

implemented into a finite element code. This kinking model is criticized and a modification is proposed for calculation of the fiber misalignment angle. The obtained results are explained for several laminates.

2. Matrix failure criteria

2.1. Matrix compressive failure criterion

Experimental results (Pinho 2005) under purely in-plane transverse compression load show that the fracture surface occurs in an angle with respect to the thickness direction as shown in Fig. 1. The experimental value for this angle is generally $\phi_o = 53^o \pm 2^o$ for most of the composite materials (Puck and Schurmann1998 and 2002).

For a general loading situation, the angle of fracture plane, ϕ, is different from the one for pure compression, ϕ_o, as shown in Fig. 2. In 3D formulation, traction components are

$$\begin{aligned} \sigma_n &= \frac{\sigma_b + \sigma_c}{2} + \frac{\sigma_b - \sigma_c}{2} Cos(2\phi) + \tau_{bc} Sin(2\phi) \\ \tau_T &= -\frac{\sigma_b - \sigma_c}{2} Sin(2\phi) + \tau_{bc} Cos(2\phi) \\ \tau_L &= \tau_{ab} Cos(\phi) + \tau_{ca} Sin(\phi) \end{aligned} \tag{1}$$

In the above equations the subscript *a* refers to the fiber direction, the subscript *b* refers to the in-plane transverse direction and the subscript c refers to the through-the-thickness direction.

The Mohr-Coulomb criterion can be expressed in several forms for matrix compressive failure. Puck and Schurmann (1998 and 2002) initially proposed the following criterion

$$f_{mc} = \left(\frac{\tau_T}{S_T - \mu_T \sigma_n}\right)^2 + \left(\frac{\tau_L}{S_L - \mu_L \sigma_n}\right)^2 = 1 \tag{2}$$

Whereas Davila *et al* (2003) proposed the following criterion

$$f_{mc} = \left(\frac{\langle |\tau_T| + \mu_T \sigma_n \rangle}{S_T}\right)^2 + \left(\frac{\langle |\tau_L| + \mu_L \sigma_n \rangle}{S_L}\right) = 1 \tag{3}$$

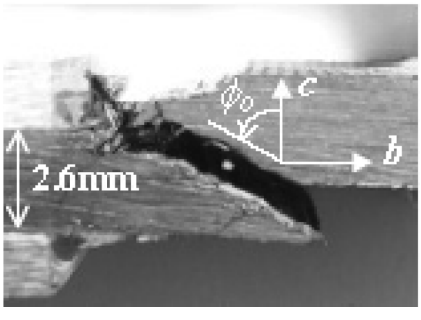

Fig. 1 Fracture surface angle for pure transverse compression loading (Pinho 2005)

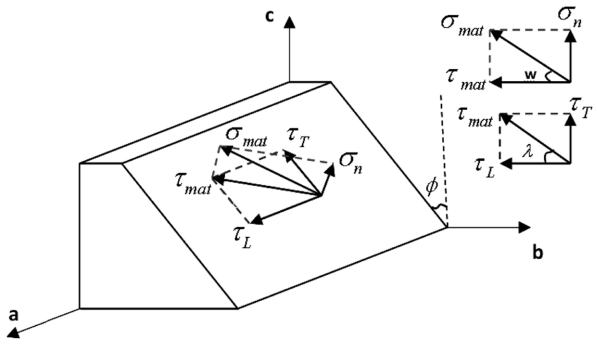

Fig. 2 Fracture surface angle for a general loading situation

Where, the operator $<\bullet>$ is the Mc-Cauley bracket defined as $<x> = \max\{o, x\}$, $x \in R$.

Puck and Schurmann (1998 and 2002) finally decided to use the following expression, believing that it fits the experimental data in better agreement

$$f_{mc} = \frac{\tau_T^2}{S_T^2 - 2\mu_T S_T \sigma_n} + \frac{\tau_L^2}{S_L^2 - 2\mu_L S_L \sigma_n} = 1 \tag{4}$$

Pinho (2005) improved Eq. (3) and obtained the following criterion

$$f_{mc} = \left(\frac{<|\tau_T| + \mu_T \sigma_n Cos(\theta)>}{S_T}\right)^2 + \left(\frac{<|\tau_L| + \mu_L \sigma_n Sin(\theta)>}{S_L}\right)^2 = 1 \tag{5}$$

Where τ_T, τ_L and σ_n are the traction components on potential fracture planes as shown in Fig. 2 and Y_t and S_L are the transverse tensile and longitudinal shear strengths, respectively. μ_T and μ_L are friction coefficients in the transverse and longitudinal directions and S_T is fracture plane resistance causes by transverse shear. The following relations between the above parameters and fracture plane angle are also defined

$$\tan(2\phi_o) = -\frac{1}{\mu_T} \tag{6}$$

$$S_T = \frac{Y_c}{2\tan(2\phi_o)} \tag{7}$$

$$\frac{\mu_L}{S_L} = \frac{\mu_T}{S_T} \tag{8}$$

Where Y_c is the transverse compressive strength.

Due to the existed simplicity in Eq. (2), it has been preferred to use by researches such as Pinho.

2.2. Matrix tensile failure criterion

For a general stress state, the quadratic interaction form between the traction components, expressed in

the potential fracture plane is considered (Pinho (2005))

$$f_{mt} = \left(\frac{\sigma_n}{Y_t}\right)^2 + \left(\frac{\tau_T}{S_T}\right)^2 + \left(\frac{\tau_L}{S_L}\right)^2 = 1 \tag{9}$$

3. Fiber-kinking failure criterion

Fiber-kinking failure usually has been observed in the high fiber-volume fraction composite materials when they are under compressive load. A schematic representation of a kink band is shown in Fig. 3. In this section, the stress based fiber-kinking model which has been proposed by Pinho (2005), with an improvement in calculation of the fiber misalignment angle is explained. In this stress based fiber-kinking model, kinking results from matrix failure mechanism in the plane parallel to the misaligned fibers or from instability mechanism due to the loss of shear stiffness for large shear strain values.

A unidirectional composite with misaligned region under compression is considered as depicted in Fig. 4. The stresses in the misalignment frame for a general plane stress loading are

$$\sigma_{a^m} = \frac{\sigma_a + \sigma_b}{2} + \frac{\sigma_a - \sigma_b}{2} Cos(2\theta) + \tau_{ab} Sin(2\theta)$$

$$\sigma_{b^m} = \frac{\sigma_a + \sigma_b}{2} - \frac{\sigma_a - \sigma_b}{2} Cos(2\theta) - \tau_{ab} Sin(2\theta)$$

$$\tau_{a^m b^m} = -\frac{\sigma_a - \sigma_b}{2} Sin(2\theta) + \tau_{ab} Cos(2\theta) \tag{10}$$

For a 2D condition under pure compression in which the matrix failure mechanism is occurred, by using the criterion in Eq. (2) the value of misalignment angle at the failure point, θ_c, is calculated from the following equation

$$X_c(Sin(\theta_c)Cos(\theta_c) - \mu_L Sin^2(\theta_c)) = S_L \tag{11}$$

Where, X_c is the axial compressive strength.

Davila *et al.* (2003) solved this equation for θ_c and found the following expression

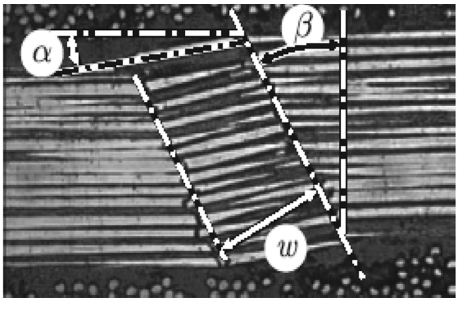

Fig. 3 Micrograph from experiments in CFRP and kink band geometric parameters (Pinho *et al.* 2006 and Pimenta *et al.* 2009)

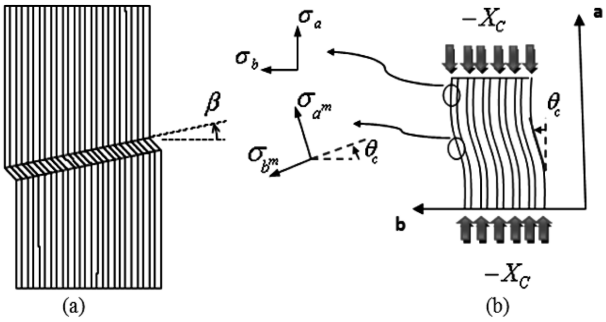

Fig. 4 (a) kink band, (b) fiber misalignment frame

$$\theta_c = arctan\left(\frac{1-\sqrt{1-4\left(\frac{S_L}{X_c}+\mu_L\right)\frac{S_L}{X_c}}}{2\left(\frac{S_L}{X_c}+\mu_L\right)}\right) \tag{12}$$

Using the shear constitutive law, the shear strain γ_{mc} can be obtained from the shear stress τ_{mc} and the initial misalignment angle, θ_i, can be calculated. From the constitutive law, the shear stress at failure point (and in the material axes) is a function of the shear strain

$$\tau_{mc} = f_{cl}(\gamma_{mc}) \tag{13}$$

For a 2D condition under pure compression, the shear stress at an angle θ_c is

$$\tau_{mc} = \frac{1}{2}Sin(2\,\theta_c)X_c \tag{14}$$

Combining of the two above equations for the shear strain at failure point in pure compression, γ_{mc}, leads to

$$\gamma_{mc} = f_{cl}^{-1}\left(\frac{1}{2}Sin(2\,\theta_c)X_c\right) \tag{15}$$

Now, the initial misalignment angle can be calculated by the following equation

$$\theta_i = \theta_c - \gamma_{mc} \tag{16}$$

In the condition that the failure occurs due to the instability mechanism, before occurrence of matrix cracking the following conditions are satisfied

$$\begin{cases} f_{CL}(\gamma_{mc}) = \frac{1}{2}Sin(2(\theta_i+\gamma_{mc}))X_c \\ \frac{\partial f_{CL}(\gamma_{mc})}{\partial \gamma_{mc}} = X_c Cos(2(\theta_i+\gamma_{mc})) \end{cases} \tag{17}$$

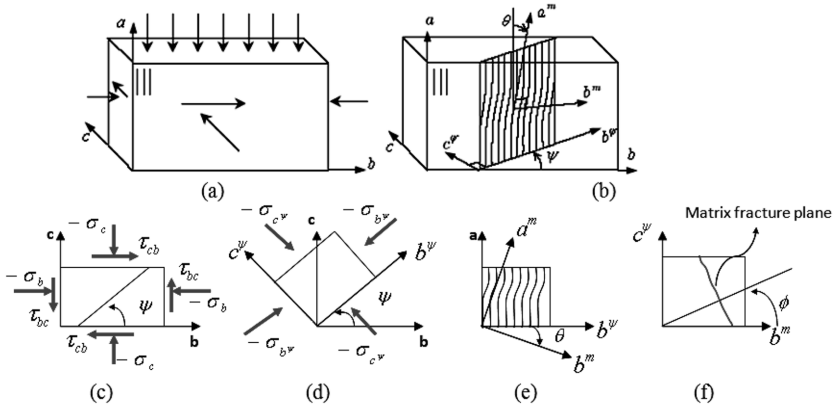

Fig. 5 3D kinking model:(a) solid under general loading condition, (b) fiber-kinking plane, (c) stresses in (a,b,c) coordinate system, (d) stresses in (a, b^{ψ}, c^{ψ}) coordinate system, (e) stresses in misalignment frame and (f) matrix failure plane (Pinho (2005))

The above equations represented that the in-plane shear stress curve and shear stress curve obtained from the stress transformation are tangent and any increasing in the load causes their divergence. By solving the Eq. (17), the initial misalignment angle of fibers and the shear strain at the failure point can be calculated.

A 3D kinking model was also proposed by Pinho (2005). A unidirectional lamina under a general compressive state of stress is considered as shown in Fig. 5(a). The fiber-kinking plane is assumed to be at an angle with the b axis (ψ), as shown in Fig. 5(b). It has been assumed that c^{ψ} and b^{ψ} are the principal directions in the b-c plane. Therefore, ψ can be calculated by the following equation (see also Fig. 5(c))

$$\tan(2\psi) = \frac{2\tau_{bc}}{\sigma_b - \sigma_c} \tag{18}$$

Eq. (19) can be used to transform the stresses to the potential fiber-kinking plane as follows

$$\begin{aligned}
\sigma_{b^{\psi}} &= \frac{\sigma_b + \sigma_c}{2} + \frac{\sigma_b - \sigma_c}{2} Cos(2\psi) + \tau_{bc} Sin(2\psi) \\
\sigma_{c^{\psi}} &= \sigma_b + \sigma_c - \sigma_{b^{\psi}} \\
\tau_{ab^{\psi}} &= \tau_{ab} Cos(\psi) + \tau_{ca} Sin(\psi) \\
\tau_{b^{\psi}c^{\psi}} &= -\frac{\sigma_b - \sigma_c}{2} Sin(2\psi) + \tau_{bc} Cos(2\psi) \\
\tau_{c^{\psi}a} &= \tau_{ca} Cos(\psi) - \tau_{ab} Sin(\psi)
\end{aligned} \tag{19}$$

The fiber misalignment angle is calculable by

$$\theta = \frac{\tau_{ab^{\psi}}}{\left|\tau_{ab^{\psi}}\right|}(\theta_i + \gamma_m) \tag{20}$$

Where, the strain γ_m is obtained by solving the following equation iteratively

$$f_{CL}(\gamma_m) = -\frac{\sigma_a - \sigma_{b^\psi}}{2} Sin(2(\theta_i + \gamma_m)) + \left|\tau_{ab^\psi}\right| Cos(2(\theta_i + \gamma_m)) \tag{21}$$

If Eq. (21) does not have a solution, then failure has taken place by instability. Then, the failure envelope for this mode is defined by

$$\begin{cases} f_{CL}(\gamma_m) = -\dfrac{\sigma_a - \sigma_{b^\psi}}{2} Sin(2(\theta_i + \gamma_m)) + \left|\tau_{ab^\psi}\right| Cos(2(\theta_i + \gamma_m)) \\ \dfrac{\partial f_{CL}(\gamma_m)}{\partial \gamma_m} = -(\sigma_a - \sigma_{b^\psi}) Cos(2(\theta_i + \gamma_m)) - 2\left|\tau_{ab^\psi}\right| Sin(2(\theta_i + \gamma_m)) \end{cases} \tag{22}$$

Now, using the misalignment angle, θ, the stresses can be transformed in to the misalignment frame as follows

$$\begin{aligned} \sigma_{a^m} &= \frac{\sigma_a + \sigma_{b^\psi}}{2} + \frac{\sigma_a - \sigma_{b^\psi}}{2} Cos(2\theta) + \tau_{ab^\psi} Sin(2\theta) \\ \sigma_{b^m} &= \sigma_a + \sigma_{b^\psi} - \sigma_{a^\psi} \\ \tau_{a^m b^m} &= -\frac{\sigma_a - \sigma_{b^\psi}}{2} Sin(2\theta) + \tau_{ab^\psi} Cos(2\theta) \\ \tau_{b^m c^\psi} &= \tau_{b^m c^\psi} Cos(\theta) - \tau_{c^\psi a} Sin(\theta) \\ \tau_{c^\psi a^m} &= \tau_{c^\psi a} Cos(\theta) + \tau_{b^m c^\psi} Sin(\theta) \end{aligned} \tag{23}$$

At this stage, the matrix failure can also be checked

$$f_{kink} = \left(\frac{\tau_T}{S_T - \mu_T \sigma_n}\right)^2 + \left(\frac{\tau_T}{S_L - \mu_L \sigma_n}\right)^2 = 1, \ \sigma_{b^m} \le \circ \tag{24}$$

$$f_{kink} = \left(\frac{\sigma_n}{Y_t}\right)^2 + \left(\frac{\tau_T}{S_T}\right)^2 + \left(\frac{\tau_L}{S_L}\right)^2 = 1 \qquad , \sigma_{b^m} > \circ \tag{25}$$

In the two above equations, the traction components on the fracture plane are given by

$$\begin{aligned} \sigma_n &= \frac{\sigma_{b^m} + \sigma_{c^\psi}}{2} + \frac{\sigma_{b^m} - \sigma_{c^\psi}}{2} Cos(2\phi) + \tau_{b^m c^\psi} Sin(2\phi) \\ \tau_T &= -\frac{\sigma_{b^m} - \sigma_{c^\psi}}{2} Sin(2\phi) + \tau_{b^m c^\psi} Cos(2\phi) \\ \tau_L &= \tau_{a^m b^m} Cos(\phi) + \tau_{c^\psi a^m} Sin(\phi) \end{aligned} \tag{26}$$

The above proposed 3D model for kinking is a stress based model and the most important parameter that must be calculated, is the misalignment angle, θ. For calculating the misalignment angle the equations must be solved iteratively. Thus Pinho considered a modification and used the following equation to calculate the misalignment angle

$$\gamma_{mi} = f_{CL}^{-1}\left(\left|-\frac{\sigma_a - \sigma_{b^\psi}}{2} Sin(2\,\theta_i) + \left|\tau_{ab^\psi}\right| Cos(2\,\theta_i)\right|\right) \tag{27}$$

In this equation, the initial misalignment angle, θ_i, is deduced from experimental data by solving the following equation iteratively

$$\theta_i = \theta_C - f_{cL}^{-1}\left(\frac{1}{2} Sin(2\,\theta_i) X_c\right) \tag{28}$$

And the misalignment angle θ becomes as

$$\theta = \frac{\tau_{ab^\psi}}{\left|\tau_{ab^\psi}\right|}(\theta_i + \gamma_{mi}) \tag{29}$$

4. Finite element implementation

4.1. Material behavior

Before the occurrence of any damage, the in-plane shear deformation is only considered to behave nonlinearly. For definition of the in-plane shear response, the maximum shear strain is defined as (Pinho (2006), Part II)

$$\gamma_{ab}^{\max}(t) = \max\{\left|\gamma_{ab(t')}\right|\}, \quad t' \le t \tag{30}$$

And the inelastic shear strain as

$$\gamma_{ab}^{in} = \gamma_{ab}^{\max} - f_{cL}(\gamma_{ab}^{\max})/G_{ab} \tag{31}$$

The function $f_{cL}(\gamma_{ab})$ represents the value of shear stress for $\gamma_{ab} \ge 0$. The material shear deformations shown in Fig. 6 can be presented as

$$\tau_{ab} = \begin{cases} \dfrac{\gamma_{ab}}{\left|\gamma_{ab}\right|} f_{CL}(\left|\gamma_{ab}\right|) & \left|\gamma_{ab}\right| = \gamma_{ab}^{\max} \\ \dfrac{\gamma_{ab}}{\left|\gamma_{ab}\right|} G_{ab}\langle\left|\gamma_{ab}\right| - \gamma_{ab}^{in}\rangle & \left|\gamma_{ab}\right| = \gamma_{ab}^{\max} \end{cases} \tag{32}$$

Where G_{ab} is the shear modulus in the (a, b) plane.

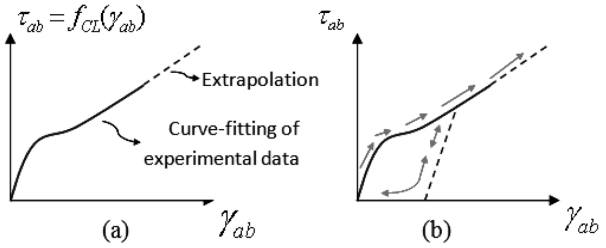

Fig. 6 (a) Typical experimental nonlinear shear behavior, (b) irreversibility: loading, unloading and reloading paths

4.2. Damage formulation

A typical unidirectional laminate loaded in transverse tension is shown in Fig. 7(a). After damage initiation, damage variable is used to explain the material behavior. In this study in order to obtain the damage variable, a bilinear softening constitutive law is assumed as shown in Fig. 7(b).

According to Fig. 7(b), the maximum strain, ε^f, can be obtained as a function of the energy per unit area of damage or fracture surfaces, Γ, material strength, σ^o, and the element dimension, L_2(Pinho (2006), Part II)

$$\varepsilon^f = \frac{2\Gamma}{\sigma^o l_2} \tag{33}$$

The damage variable, d, is defined to consider a linear degradation for the relevant stress components. The instantaneous value of the damage variable, d^{inst}, is also defined as

$$d^{inst} = max\left\{0, \min\left\{1, \varepsilon^f \frac{\varepsilon - \varepsilon^o}{\varepsilon(\varepsilon^f - \varepsilon^o)}\right\}\right\} \tag{34}$$

Considering the irreversibility condition, the damage variable is defined as

$$d(t) = \max\{d^{inst}(t')\}, t' \le t \tag{35}$$

4.2.1. Matrix failure modeling

In this damage mode when the matrix failure criterion is satisfied, the traction components on the

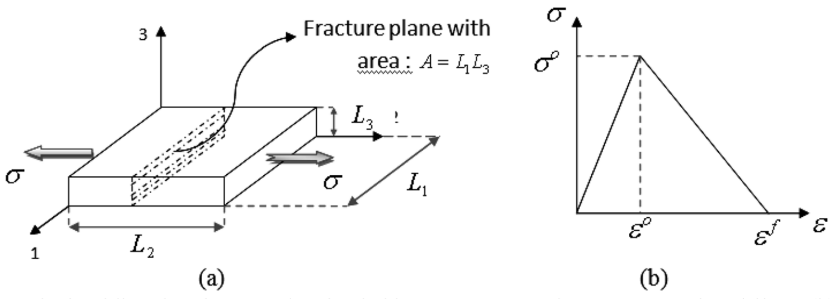

Fig. 7 (a) Typical unidirectional composites loaded in transverse tension up to complete failure, (b) Material constitutive law with linear softening

fracture plane are degraded

$$\tau_T \leftarrow (1 - d_{mat})\,\tau_T,\quad \tau_L \leftarrow (1 - d_{mat})\,\tau_L,\quad \sigma_n \leftarrow \left(1 - d_{mat}\frac{<\sigma_n>}{\sigma_n}\right)\sigma_n \tag{36}$$

To derive the damage variable, the strain variable, ε_{mat}, the magnitude of traction on the fracture plane, σ_{mat}, and the characteristic length, L_{mat}, have to be calculated. The magnitude of traction on the fracture plane is (see Fig. 2)

$$\sigma_{mat} = \sqrt{<\sigma_n>^2 + \tau_{mat}^2} \tag{37}$$

In which the shear component, τ_{mat}, defined as

$$\tau_{mat} = \sqrt{\tau_T^2 + \tau_L^2} \tag{38}$$

The elastic strain components on the fracture plane are

$$\begin{aligned}
\varepsilon_n &= \frac{1}{2}[(\varepsilon_b + \varepsilon_c) + (\varepsilon_b - \varepsilon_c)Cos(2\phi) + \gamma_{bc}Sin(2\phi)] \\
\gamma_T &= -(\varepsilon_b - \varepsilon_c)Sin(2\phi) + \gamma_{bc}Cos(2\phi) \\
\gamma_L^{eL} &= \gamma_{ab}^{eL}Cos(\phi) + \gamma_{ca}Sin(\phi)
\end{aligned} \tag{39}$$

Where the elastic component of the in-plane shear strain is

$$\gamma_{ab}^{eL} = \frac{\tau_{ab}}{G_{ab}} \tag{40}$$

It is notable that the elastic internal energy in the element at the onset of failure is only contributed to the fracture process. Therefore, the elastic part of γ_{ab} is only considered. The strain acting on the direction of σ_{mat} is defined as

$$\varepsilon_{mat} = \frac{<\sigma_n>}{\sigma_n}\varepsilon_n Sin(\omega) + \gamma_{mat}Cos(\omega) \tag{41}$$

Where

$$\begin{aligned}
\gamma_{mat} &= \left|\gamma_T Gos(\lambda) + \gamma_L^{eL}Sin(\lambda)\right| \\
\lambda &= \arctan\left(\frac{\tau_L}{\tau_T}\right), \quad w = \arctan\left(\frac{<\sigma_n>}{\tau_{mat}}\right)
\end{aligned} \tag{42}$$

The onset stress and strain are determined from the value of σ_{mat} and ε_{mat} at the onset of failure

$$\sigma_{mat}^{\circ} = \sigma_{mat}\big|_{F_{mat=1}},\quad \varepsilon_{mat}^{\circ} = \varepsilon_{mat}\big|_{F_{mat-1}} \tag{43}$$

Finally, the expression for ε_{mat}^{f} is

$$\varepsilon_{mat}^{f} = \frac{2\Gamma}{\overset{\circ}{\sigma}_{mat} L_{mat}} \tag{44}$$

The characteristic length, L_{mat}, is defined as

$$L_{mat} = \frac{L_1 L_2 L_3}{L_a L_{c^{\phi}}} \tag{45}$$

The required variables to define the L_{mat} are introduced in Fig. 8.

In particular, if no mixed mode data is known, a simple weighted average of Γ_b, Γ_T and Γ_L can be used to determine the fracture toughness, Γ.

$$\Gamma = \Gamma_b \left\langle \frac{\overset{\circ}{\sigma}_n}{\overset{\circ}{\sigma}_{mat}} \right\rangle + \Gamma_T \left(\frac{\overset{\circ}{\tau}_T}{\overset{\circ}{\sigma}_{mat}} \right)^2 + \Gamma_L \left(\frac{\overset{\circ}{\tau}_T}{\overset{\circ}{\sigma}_{mat}} \right)^2 \tag{46}$$

Where Γ_b is the mode-I interalaminar fracture toughness and $\Gamma_T = \Gamma_L = G_{IIC}$ (Puck and Schurmann 1998).

4.2.2. Modeling of fiber-kinking failure mode

After satisfaction of Eq. (24) or (25) and kinking failure initiation, the shear stresses on the kink band ($\tau_{C^{\psi}a^m}$, $\tau_{a^m b^m}$) as well as the stress normal to the kink band (depending on the sign of σ_{a^m}) are degraded using the damage variable, d_{kink}

$$\tau_{a^m b^m} \leftarrow (1 - d_{kink})\, \tau_{a^m b^m}, \quad \tau_{c^{\psi} a^m} \leftarrow (1 - d_{kink})\, \tau_{c^{\psi} a^m}, \quad \sigma_{a^m} \leftarrow \left(1 - d_{kink} \frac{\langle \sigma_{a^m} \rangle}{\sigma_{a^m}}\right) \sigma_{a^m} \tag{47}$$

This failure process is associated with the rotation of the fibers in the kink band, which is due to the

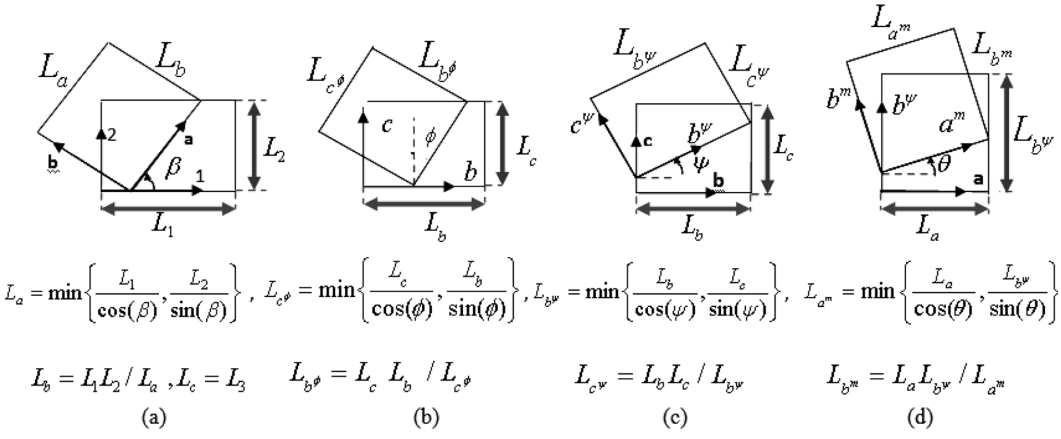

Fig. 8 Determination of the characteristic length within an element: (a) Rotation of an angle β, (b) rotation of an angle ϕ, (c) Rotation of an angle ψ, (d) rotation of an angle θ

shear stress, $\tau_{a^m b^m}$. Therefore at the scale of the kink band, failure propagation is controlled by the driving stress, $\sigma_{kink} = \tau_{a^m b^m}$. Also, in this mode, the elastic component of γ_{ab}, ($\gamma_{ab}^{eL} = \frac{\tau_{ab}}{G_{ab}}$), is only considered for the driving strain, which is defined as $\varepsilon_{kink} = \gamma_{a^m b^m}^{eL}$, where $\gamma_{a^m b^m}^{eL}$ is obtained by rotation of the elastic strains.

The onset stress and strain are defined as

$$\overset{\circ}{\sigma}_{kink} = |\sigma_{kink}|_{f_{kink}=1}, \overset{\circ}{\varepsilon}_{mat} = |\varepsilon_{kink}|_{f_{kink}=1} \tag{48}$$

And the expression for the final strain ε_{kink}^{f} is

$$\varepsilon_{kink}^{f} = \frac{2\Gamma_{kink}}{\overset{\circ}{\sigma}_{kink} L_{kink}} \tag{49}$$

The characteristic length L_{kink} in the above equation shown in Fig. 8 is defined as

$$L_{kink} = \frac{L_1 L_2 L_3}{L_{a^m} L_{c^\psi}} \tag{50}$$

Finally, the fracture toughness or energy density for kinking, Γ_{kink}, can be obtained from the experiments (Pinho *et al*. 2006).

5. Modification and improvement

In the previously proposed stress based kinking model the shear stress constitutive law which is used in the global frame (Eq. (32)) will be used in the local frame (misalignment frame) to calculate the misalignment angle (Eq. (21)). In this paper, calculation of misalignment angle of fibers, θ, is improved on the base of strains and implemented into an explicit finite element code (Abaqus). It is worth to note that the strains in each increment are usually available, therefore implementation of models based on the strains are easier than those based on the stresses. In order to calculate the misalignment angle at failure, θ_c, initial misalignment angle, θ_i, and the fiber-kinking plane, Eqs. (12), (16) and (18) are used. Now, the important parameter of misalignment angle, θ, can be calculated using the following equation

$$\theta = \theta_i + \gamma_m \tag{51}$$

In which, θ_i is a material parameter and can be positive or negative and γ_m is the shear strain in the misalignment frame which can be determined as

$$\varepsilon_{b^\psi} = \frac{1}{2}(\varepsilon_b + \varepsilon_c + (\varepsilon_b - \varepsilon_c)\cos(2\psi) + \gamma_{bc}\sin(2\psi)) \tag{52}$$

$$\gamma_{ab^\psi} = \gamma_{ab}\cos(\psi) + \gamma_{ca}\sin(\psi) \tag{53}$$

$$\gamma_m = -(\varepsilon_a - \varepsilon_{b^\psi})\sin(2\theta_i) + \gamma_{ab^\psi}\cos(2\theta_i) \tag{54}$$

After calculation of the misalignment angle, θ, the stress components in the misalignment frame can be determined using Eqs. (19) and (23). At this stage, the matrix failure is checked using the criteria defined by Eqs. (24) and (25) which in these equations the traction components on the fracture plane are determined by Eq. (26). The angle ϕ is obtained by trying a small number of tentative angles in the interval of $0 \leq \phi < \pi$.

In the proposed modification, only the process of fiber misalignment angle calculation is considered. However, similar to the stress based fiber kinking model, the improvement can be applied to other steps of the procedure such as fracture surface selection and stress calculations.

6. Numerical results

The carbon/epoxy material properties used for numerical analysis are shown in Table 1. The available experimental in-plane shear stress versus strain behavior (Pinho 2005) was used in the numerical analysis. This behavior has been fitted by the logarithmic function of, $k_1 \ln(k_2\gamma + 1)$ with $k_1 = 46$ and $k_2 = 100$. The fracture angle for pure transverse compression is considered as $\phi_0 = 53^o$. Regarding the through-the-thickness direction, it is assumed that the composite material behave transversely isotropic and the interlaminar toughness is $\Gamma_b = 0.22 kj/m^2$, the parameter Γ_{kink} is 79.9 kj/m^2 and $\Gamma_L = \Gamma_T = 1.1$ kj/m. (Pinho (2005)).

In the above table, E_a, E_b and, G_{ab} are the elastic modulus in the fiber direction, the elastic modulus in the transverse direction and the shear modulus in the (a, b) plane respectively and Y_t, Y_c, X_c, X_t, S_{ab} are the tension and compressive strength in the transverse direction, compressive and tension strength in the fiber direction and shear strength in the plane (a, b) respectively and ν_{bc} and ν_{ba} are the poison ratios.

6.1. Matrix failure under purely in-plane transverse compression load

For verifying the matrix failure model implemented into the finite element code, a numerical analysis is carried out. For this purpose a model with 60 mm length, 15 mm width and 10 mm thickness and material properties mentioned in Table 1, is generated and transversely loaded until damage process is completed. In the plane of lamina, element size should be small enough to ensure that the characteristic length, L_{mat} in Eq. (45), is adequate for calculating of ε_{mat}^{f} in Eq. (44). In this model the in-plane element size is considered to be about 0.6 mm. A typical fracture surface obtained from pure transverse compression test has been shown in Fig. 1. The experimental fracture surface has an angle of about 53° from the thickness direction. The results of numerical analysis also have been shown in Figs. 9(a) and (b). The angle of the failure band which can be observed in the model is between 51°-54° which is in good agreement with the previously obtained experimental results.

For a further verification, the authors carried out purely in-plane transverse compression experiments on specimens made by Glass/Epoxy (Type C) ASNA 4197 Prepreg unidirectional composite. The specimens had 13.6 mm length, 9.8 mm width (in the fiber direction) and 6 mm thickness approximately. In order to ensure that the specimens are in full contact with the loading devices and to eliminate the potential bending

Table 1 Material properties for T300/913 (Pinho 2005)

Material properties	E_a(GPa)	E_b(GPa)	G_{ab}(GPa)	Y_t(MPa)	Y_c(Mpa)	X_c(MPa)	X_t(MPa)	S_{ab}(MPa)	ν_{bc}	ν_{ba}
T300/913	132	8.8	4.6	68	198	1355	2005	150	0.4	0.021

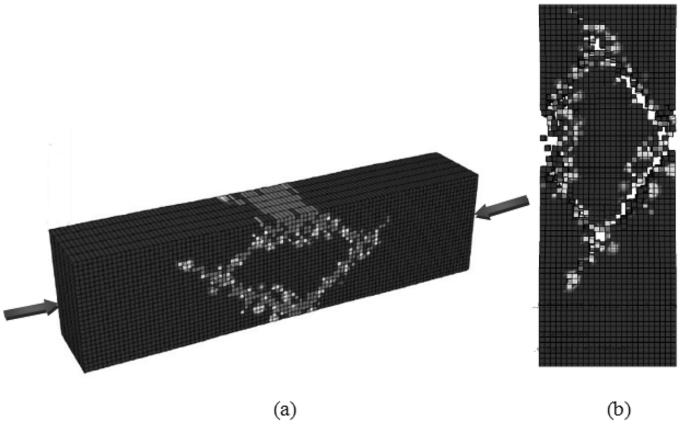

Fig. 9 (a) Numerical results for matrix failure under purely in-plane transverse compression load, (b) present the results after eliminating of the damaged elements

moments, a spherical self adjusting device (similar to Bing and Sun work (2008)) was manufactured and used.

The obtained experimental results are shown in Fig. 10. The fracture surface angle is measured between 49° to 58° with an average of 53.8° through the thickness which is closed to that found by others for Carbon/Epoxy composite (see Fig. 10(a)). The obtained experimental transverse compressive strength of Glass/Epoxy (Type C) ASNA 4197 specimens was about 125 MPa.

6.2. Shear failure modeling of (±45)s test specimen

Pinho (2005) carried out shear tests with (±45)8s lay-ups (zero fiber angle is in loading direction) according to the ASTM standard D3518/D3518M-01 and found ±45° failure band as shown in Fig. 11(a). Numerical analyses of different models shown that the fracture surface prediction may be independent of the dimensions and number of lay-ups (n in (±45)ns) of finite element model. The presented material properties in Table 1 were also used for this numerical analysis.

In Figs. 11(a), (b), (c) and (d) the ±45° failure band can be observed which are in good agreement with

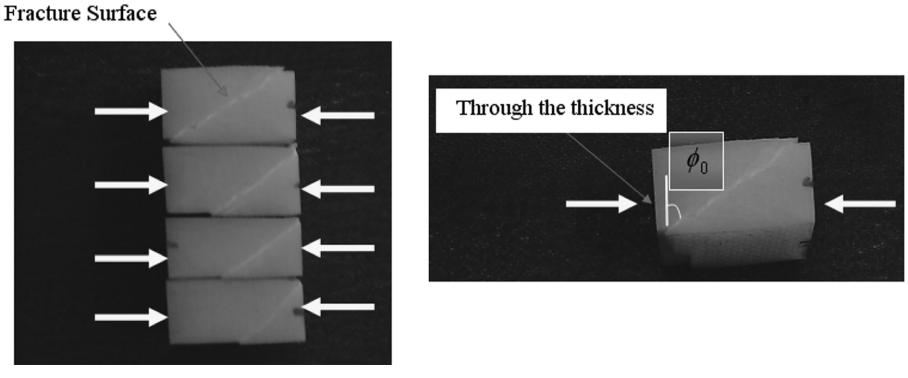

Fig. 10 Fracture surface angles for transversely compression tests on Glass/Epoxy (Type C) ASNA 4197 composite

the experimental results. In the numerical model shown in Fig. 11 no effort is carried out to specify the failure initiation point. The results show that the failure is initiated from the edges. However, if the weekend element or pre-crack is used to specify the failure initiation point, the ±45° failure band will be observed as shown in Fig. 12. In Fig. 12, the model has a pre-crack in the middle and a quarter of the model is used for symmetry.

In order to investigate the failure of woven composite laminates, the authors performed similar experiments for this type of laminates. The specimens were made by hand lay-up technique with 8 layer Eglass-polyester (marine grade) material. The size of the specimens selected according to the ASTM standard D3039/D3039M-00 and depicted in Table 2. The specimens were manufactured with fibers directions of ±45°, similar to the specimen shown in Fig. 11(a). Figs. 13(a), (b) and (c) show the specimens before and after testing.

As shown in Figs. 13(b) and (c) the angle of failure band is about 45° and similar behavior for these two types of composites ((±45)s unidirectional laminated composite and woven laminated composite) has been observed.

6.3. Fiber compression failure modeling

In this section, the formation of kink-bands is predicted using the two explained stress based and strain based failure models. For T300/913 composite laminate, Pinho observed that the kink band is formed within 25±5° for standard axial compression specimens (see Fig. 14(a)). A numerical model with 10 mm length, 10 mm width and 2 mm thickness is used for this analysis. The obtained results from the implementation of stress based failure model for the failure analyses of T300/913 composite laminates are

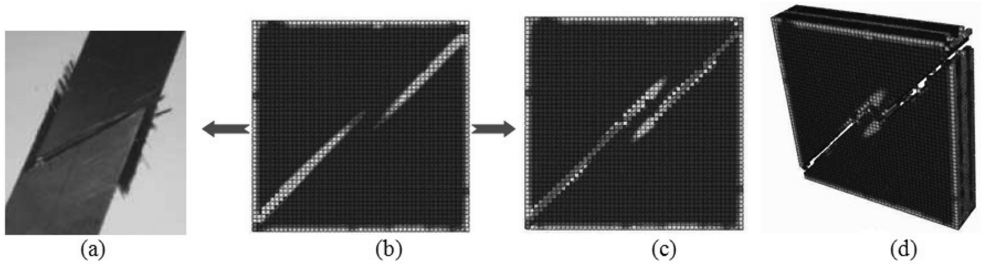

Fig. 11 (a) shear test specimen (Pinho 2005), (b) model of shear specimen, (c) prediction of 45° failure band in with $(\pm 45)_{8s}$ model, (d) the result of matrix failure after eliminating the damaged elements

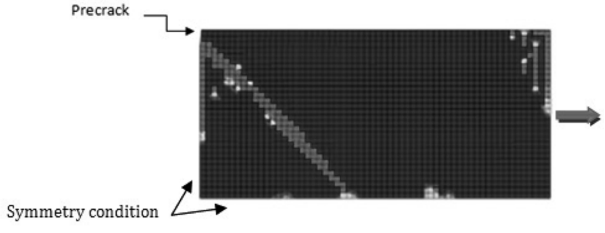

Fig. 12 ±45° failure band observation in numerical analysis with the model which has a precrack (a quarter of the model is shown for symmetry)

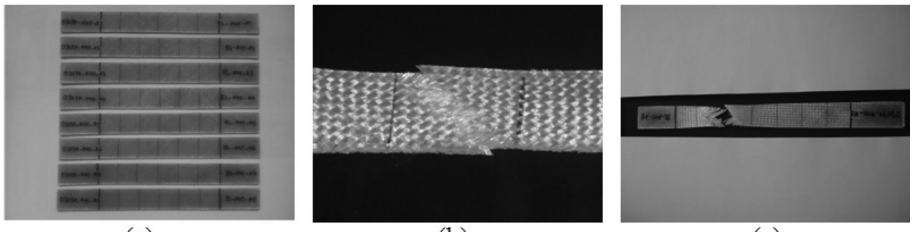

(a) (b) (c)

Fig. 13 (a) test specimens, (b) the obtained failure band during the test, (c) test specimen after failure

Table 2 Nominal dimensions of specimens

Overall length (mm)	Average thickness (mm)	Average width (mm)
250	2.5	25

depicted in Fig. 14. It is worth to note that updating of the misalignment frame after damage initiation in this type of modeling leaded to the less accurate results. Therefore, the analyses were performed without updating the misalignment frame. The obtained kink-band angle for this stress based failure model is between 18º to 20º, however Pinho *et al*. (2006) reported that about 15º in numerical analyses.

The implemented strain based model into the finite element code is also used for the analyses of the same laminate. The misalignment frame updating is easer here because the formulation of the strain based model is simpler than the stress based one. Therefore, the numerical analyses for this model were performed with the misalignment frame updating after damage initiation. Fig. 15 shows that the obtained kink-band angle is between 20º to 23º which is in better agreement with the experimental result when compared with the stress based fiber kinking model (Pinho 2005). Similar to the stress based model, some failure scattering is observed in the results which can be improved by updating the fracture surface and stress in every step of the procedure (Section 5).

In another attempt, the mesh dependency of kink-band formation is also examined for stress based model. For this purpose, the model with $10 \times 10 \times 2$ mm in dimensions is analyzed using three different meshes with the elements size of $0.4 \times 0.4 \times 0.4$ mm (coarse), $0.2 \times 0.2 \times 0.2$ mm (medium) and $0.1 \times 0.1 \times 0.2$ mm (fine). The results for kink-band width and kink-band angle are shown in Fig. 16. The strength and kink-band angle predictions are not significantly changed between these three models. However more kink-band scattering is observed as the mesh becomes finer.

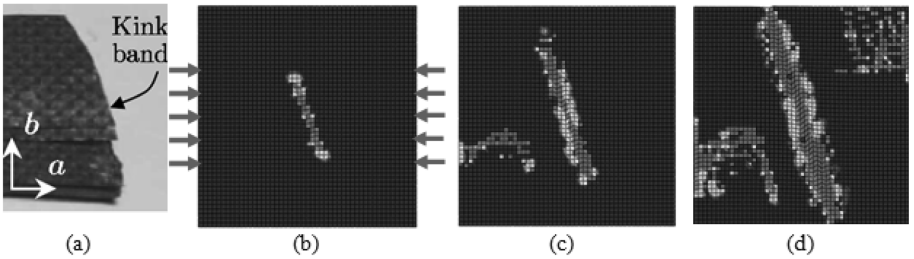

(a) (b) (c) (d)

Fig. 14 (a) kink-band in the failed longitudinal compression test specimen (Pinho 2005), (b) initial kink-band angle about 20º for stress based kinking model, (c) propagation of kink-band with an angle of about 20º, (d) kink-band broadening with an angle about 18º(stress-based model)

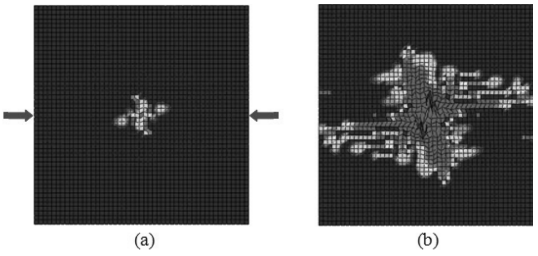

Fig. 15 Strain based model results (a) initial kink-band angle about 23°, (b) propagation of kink-band with an angle of about 20°.

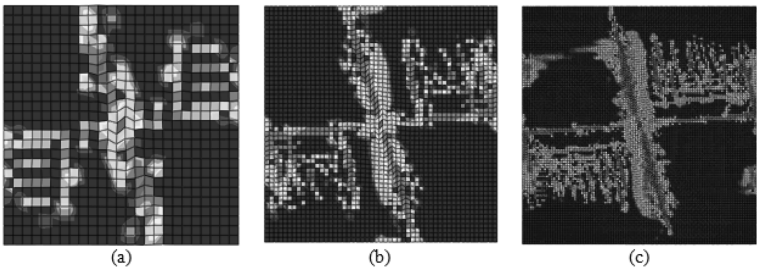

Fig. 16 (a) fiber-kinking analysis with coarse mesh, (b) medium mesh and (c) refined mesh (stress-based model)

The results of these two models are different in displacement which causes the initiation of kinking failure process. Furthermore, their damage variable contours are not similar and their predicted kink-band angles are also different (see Figs. 14 and 15). Therefore, more experimental and numerical investigations on the effects of various parameters on kink-band formation are required to evaluate these models.

7. Conclusions

From the results of this research, the following conclusions are obtained:

- The investigated matrix failure models predict the failure band angle in compression efficiently. The result of numerical analysis showed that the failure band angle predicted by these models is in good agreement with the experimental results.
- The experiments carried out on the woven laminated composite showed that the behavior of these kind of composites are similar to the unidirectional laminated composites in matrix failure mode, therefore the matrix failure models which are used for unidirectional laminated composites can be improved for the woven laminated composites failure.
- The experiments carried out on glass and carbon fiber reinforced composites showed that these two composite materials fail through the same mechanisms, and the same failure models can be used for both materials.
- The stress based kinking model proposed by Pinho (2005) can predict kink-band angle approximately. This model, without updating the misalignment frame, gives better contour for damage variable in the numerical analysis.
- Investigation of element size affection for the stress based model shown that the compressive strength

and kink-band angle predictions are not significantly changed with different element sizes. However, more kink-band scattering is observed as the mesh becomes finer.

- The strain based model proposed in this research can also predict kink-band angle approximately, but compared to the stress based one, it is simpler and with updating the misalignment frame, the results are in better agreement with the experimental results when compared with those obtained from the stress based model but failure scattering in the numerical results shows that the model needs to be improved.

References

Argon, A. S. (1972), Fracture of composites, in: Treatise on Materials Science and Technology, Academic Press, New York, 79-114.

ASTM Standard D3518/D3518M,(2001), Standard test method for in-plane shear reponse of polymer matrix composite materials by tensile test of a +/– 45 laminate, (2001).

ASTM Standard D3039/D3039M-00, Standard test method for tensile properties of polymer matrix composite materials, (2000).

Budiansky, B. (1983), "Micromechanics", Computers and Structures **16**(1-4), 3-12.

Budiansky, B. and Fleck, N. A. (1993), "Compressive failure of fibre composites", *J. Mec. Phys. Soli.* **41**(1), 183-211.

Budiansky, B., Fleck, N. A. and Amazigo , J. C. (1998), "On kink-band propagation in fiber composites", *J. Mech. Phys. Solid*, **46**(9), 1637-1653.

Bing, Q. and Sun, C.T. (2008), Specimen size effect in off-axis compression tests of fiber composites, *Comp. Eng*., Part B **39**(1), 20-26.

Christensen, R. M. and Deteresa , S. J. (1997), "The kink band mechanism for the compressive failure of fiber composite materials", *J. Appli. Mech.*, **64**(1).

Dávila, C. G., Jaunky , N. and Goswami, S. (2003), "Failure criteria for FRP laminates in plane stress", in: 44th AIAA/ASME/ASCE/AHS/ASC Structures, Structural Dynamics, and Materials Conference, AIAA Paper 1991-2003.

Dávila, C. G. and Camanho, P. P. (2003), "Failure criteria for FRP laminates in plane stress", Tech. Rep. NASA/TM-2003-212663, National Aeronautics and Space Administration, U.S.A.

Davis Jr, J. G. (1975), "Compressive strength of fiber-reinforced composite materials", in: Composite Reliability, ASTM STP 580, Americal Society for Testing and Materials, Philadelphia, 364-377.

De Ferran, M. E. and Harris, B. (1970), "Compression strength of polyester resin reinforced with steel wires", *J. Comp. Mat*, **4**(1), 62-72.

Kyriakides, S., Arseculeratne, R. and Perry, E. J. (1995), "On the compressive failure of fiber reinforced composites", *Inter. J. Solids. Struct.*, **32**(6/7), 689-738.

Lager, J. R. and June, R. R. (1969), "Compressive strength of boron-epoxy composites", *J. Comp. Mater.* **3**(1), 48-56.

Liu, D., Fleck , N. A. and Sutcliffe, M. P. F. (2004), "Compressive strength of fiber composite with random fiber waviness", *J. Mech. Phys. Solid* **52**(7), 1481-1505.

Puck, A. and Schurmann, H. (1998), "Failure analysis of FRP laminates by means of physically based phenomenological models", *Comp. Sci.Techno.* **58**(7), 1045-1067.

Puck, A. and Schurmann, H. (2002), "Failure analysis of FRP laminates by means of physically based phenomenological models", *Comp. Science. Techno.* **62**(12-13), 1633-1662.

Pinho, S.T. (2005), "Modelling failure of laminated composites using physically-based failure models", Imperial College London.

Pinho, S. T., Robinson, P. and Iannucci, L. (2006), "Fracture toughness of the tensile and compressive fiber failure modes in laminated composites", *Comp. Science . Techno.*, **66**(13), 2069-2079.

Pinho, S.T., Iannucci, L. and Robinson, P. (2006), "Physically based failure models and criteria for laminated fibre-reinforced composites with emphasis on fibre kinking. Part II: FE implementation, Applied science and manufacturing", **37**(1), 766-777.

Pimenta, S., Gutkin, R., Pinho, S. T. and Robinson P. (2009), "A micromechanical model for kink-band formation:

Part II- Analytical modeling", *Compo. Sci. Techno*, 69(7-8), 956-964.

Rosen, V. W. (1965), "Mechanics of composite strengthening", Fiber Composite Materials American Society of Metals, Metals Park, Ohio 37-75.

Schultheisz, C. R. and Waas, A. M. (1996), "Compressive failure of composites", part I: Testing and micromechanical theories, Progress in Aerospace Sciences **32**(1), 1-42.

Shuart, M. J. (1989), "Failure of compression-loaded multidirectional composite laminates", *AIAA Journal* **27**, 1274-1279.

Singh, S.B. and Kumar, Dinesh (2010), "Postbuckling response and failure of symmetric laminated plates with rectangular cutouts under in-plane shear", Structural Engineering and Mechanics, An Int\'l Journal **34**(2).

CC